

Noncovalent Interactions

Engineering Crystals Using sp^3 -C Centred Tetrel Bonding Interactions

Julius J. Roeleveld,^[a] Siebe J. Lekanne Deprez,^[a] Abraham Verhoofstad,^[a] Antonio Frontera,^[b] Jarl Ivar van der Vlugt,^[a, c] and Tiddo Jonathan Mooibroek^{*[a]}

Abstract: 1,1,2,2-Tetracyanocyclopropane derivatives **1** and **2** were designed and synthesized to probe the utility of sp^3 -C centred tetrel bonding interactions in crystal engineering. The crystal packing of **1** and **2** and their 1,4-dioxane cocrystals is dominated by sp^3 -C(CN)₂...O interactions, has significant C...O van der Waals overlap (≤ 0.266 Å) and DFT calculations indicate interaction energies of up to -11.0 kcal mol⁻¹. A cocrystal of **2** with 1,4-thioxane reveals that the cyclopropane synthon prefers interacting with O over S. Computational analyses revealed that the electropositive C₂(CN)₄ pocket in **1** and **2** can be seen as a strongly directional 'tetrel-bond donor', similar to halogen bond or hydrogen bond donors. This disclosure is expected to have implications for the utility of such 'tetrel bond donors' in molecular disciplines such as crystal engineering, supramolecular chemistry, molecular recognition and medicinal chemistry.

pane synthon prefers interacting with O over S. Computational analyses revealed that the electropositive C₂(CN)₄ pocket in **1** and **2** can be seen as a strongly directional 'tetrel-bond donor', similar to halogen bond or hydrogen bond donors. This disclosure is expected to have implications for the utility of such 'tetrel bond donors' in molecular disciplines such as crystal engineering, supramolecular chemistry, molecular recognition and medicinal chemistry.

Introduction

Phenomena such as host-guest complexation, molecular aggregation, crystallization and protein folding are often largely driven by non-covalent interactions.^[1] Such interactions include hydrogen and halogen bonding,^[1a,2] which have recently been contextualized as examples of so-called 'σ-hole interactions'.^[3] A σ-hole can be seen as region of electropositive potential along the vector of a covalent bond. The location of this potential coincides with the σ* orbital of that bond. The ultimate conclusion of a strong σ-hole donor-acceptor interaction can be the breaking and/or making of a σ bond, such as in the reaction of I₂ with I⁻ to form [I₃]⁻.^[4] In principle, each non-metal-

lic element of the periodic table could be involved in σ-hole interactions, provided the atom is placed in the appropriate molecular framework. For example: sulfur^[5] atoms in dithienothiophenes^[6] have been utilised as σ-hole donors in catalysis,^[7] to realise anion transport over membranes,^[8] and as a design element in mechanosensitive fluorescent probes.^[9]


To date, a notable absentee among the non-metal elements that have been rationally exploited as σ-hole donor is carbon,^[1b,10] which is ubiquitously present in synthetic chemistry and of central importance to life. Carbon-centred interactions with carbonyls are well established,^[11] and interactions between (coordinated) acetonitrile,^[12] carbon monoxide^[13] and carbon dioxide^[14] with appropriate acceptors have also been reported. However, these involve sp^2 - or sp -hybridized carbon atoms that do not align with the definition of a σ-hole interaction (but rather some type of π-interaction). Interestingly, polar interactions with sp^3 -hybridized carbon atoms can persist with methyl groups in crystal structures.^[15] Moreover, bonding interactions with sp^3 carbon are implicated in the 'advent' complex^[1b,4b] of canonical S_N2 nucleophilic displacement reactions, such as [Cl⁻...CH₃I]⁻ upon the attack of Cl⁻ on iodomethane.^[4b,16] In analogy to the halogen, chalcogen and pnictogen bonding nomenclature,^[17] such interactions can be termed a 'tetrel bonding interaction'.^[18]


A supramolecular synthon that would allow for predictable and directional sp^3 -C centred tetrel bonding interactions has not been experimentally established to date. Aided by computational insights, we predicted that the sp^3 hybridized C(CN)₂ centres^[19] present in 1,1,2,2-tetracyanocyclopropane (TCCP) could be a suitable and sterically accessible σ-hole.^[20] We recently reported that the sp^3 -carbon tetrel bonding potential of dimethyl-TCCP allows for supramolecular adduct formation with the electron-rich O-atom of tetrahydrofuran, both in the solid state and in the gas phase.^[21]


[a] J. J. Roeleveld, S. J. Lekanne Deprez, A. Verhoofstad, Prof. Dr. Ir. J. I. van der Vlugt, Dr. T. J. Mooibroek van 't Hoff Institute for Molecular Sciences Universiteit van Amsterdam Science Park 904, 1098 XH Amsterdam (The Netherlands) E-mail: t.j.mooibroek@uva.nl

[b] Prof. Dr. A. Frontera Department of Chemistry Universitat de les Illes Balears Crta de Valldemossa km 7.5, 07122 Palma de Mallorca (Balears) (Spain)

[c] Prof. Dr. Ir. J. I. van der Vlugt Institute of Chemistry Carl von Ossietzky University Oldenburg Carl-von-Ossietzky-Straße 9–11, 26219 Oldenburg (Germany)

 Supporting information and the ORCID identification number(s) for the author(s) of this article can be found under: <https://doi.org/10.1002/chem.202002613>.

 © 2020 The Authors. Published by Wiley-VCH Verlag GmbH & Co. KGaA. This is an open access article under the terms of Creative Commons Attribution NonCommercial License, which permits use, distribution and reproduction in any medium, provided the original work is properly cited and is not used for commercial purposes.

 Part of a Special Collection to commemorate young and emerging scientists. To view the complete collection, visit: Young Chemists 2020.

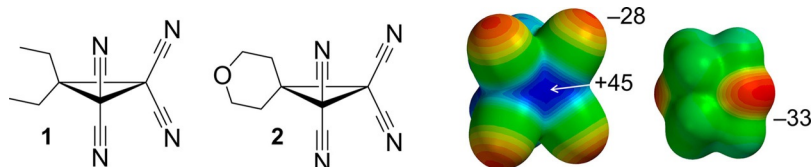


Figure 1. Molecular structures of **1** and **2**, together with a Molecular Electrostatic Potential map (MEP) of **2** and 1,4-dioxane calculated at the DFT/B3LYP-D3/def2-TZVP level of theory. The MEP is colour coded from electro-positive (blue) to electronegative (red) and the indicated potentials are in kcal mol⁻¹.

Here, we exploit and extend on this principle by demonstrating crystal engineering with sp³-C tetrel bonding interactions using TCCP derivatives **1** and **2** (Figure 1).

Compound **1** is the bulkier ethyl-derivative of the previously exploited dimethyl-TCCP.^[21] Cyclopropane **2** can be seen as a cyclic ether analogue of **1**, and was designed to combine a σ -hole donor and acceptor within the same molecule. The Molecular Electrostatic Potential map (MEP) of **2** shown in Figure 1 clearly illustrates that the cyclopropane ring of **2** bears the large positive potential (a sort of hybrid of two σ -holes) located on the sp³ C₂(C≡N)₂ atoms (the MEP of **1** is comparable). An interesting feature is that the σ -hole is observed at the middle of the C–C bond rather than two distinct σ -holes opposite to the C–C bonds, thus showing that the individual areas of depleted electron density overlap and merge.^[20a,22] It is worth mentioning that this potential is in-between the calculated potential on the H-atoms in water (+55 kcal mol⁻¹) and ammonia (+35 kcal mol⁻¹) when computed at the same level of theory.^[21] The MEP of 1,4-dioxane shown in Figure 1 illustrates the electronegative potential on the O-atoms of cyclic ethers such as **2**, which are thus anticipated to engage in directional sp³-C...O interactions. Here we confirm this hypothesis by disclosing the crystal structures of **1**, **2**, [1...dioxane], [2...dioxane] and [2...thioxane] and show that their packing is dominated by the anticipated sp³-C...O interactions.

Results and Discussion

TCCP derivatives **1** and **2** are both synthetically accessible in moderate to decent yields (34–58%) using a straightforward modified literature procedure (see experimental and ESI for full details and characterization).^[21] Single crystals suitable for X-ray diffraction measurements (see experimental for details) were obtained by slow evaporation of a solution of **1** or **2** in dichloromethane. The atomic coordinates contained within the unit cells are shown in Figure 2a and b for **1** and **2**^[23] respectively (see experimental for full details). Optimization of **1** at the B3LYP^[24]-D3^[25]/def2-TZVP^[26] level theory accurately reproduced the crystal structure coordinates of **1** (Figure S5a).

The intramolecular distances and angles measured within these structures (not shown) can be seen as normal.^[27] The crystal packing of **1** is organized by stacks of nitrile...nitrile interactions (Figure S5b). However, geometry optimization of a [1...1] dimer extracted from the crystal structure ($\Delta E^{\text{BSSE}} = -4.8$ kcal mol⁻¹) converged in a rather different ordering that is more tightly packed ($\Delta E^{\text{BSSE}} = -7.8$ kcal mol⁻¹, see Figure S5c).

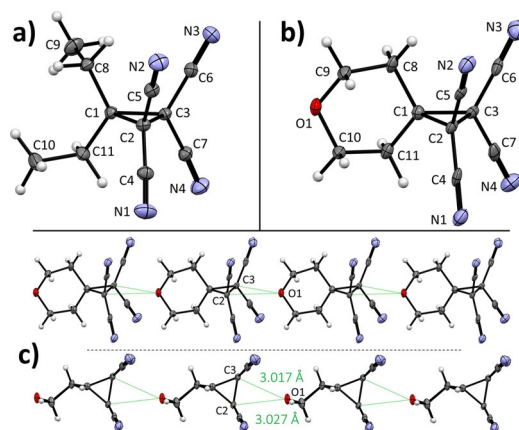


Figure 2. Single crystal X-ray diffraction structures of **1** (a) and **2** (b). c) infinite 1-dimensional pillars of **2** observed in the crystal structure, held together by short sp³ C...O contacts as shown by the two perspective views. Only distances involving the cyclopropane C-atoms are shown (green dotted lines). For more illustrations of crystal packing and a comparison to DFT optimized geometries, see Figures S5–S8. Nitrogen = blue, oxygen = red and hydrogen = white.

Also, the sp³-C...N distance elongated from 3.178 Å in the crystal structure to 3.255 Å in the DFT calculation. As with **1**, the atomic coordinates found for **2** were accurately reproduced by DFT (Figure S6b). In stark contrast with the packing obtained for **1**, crystal packing of the unit cell for species **2** (Figure 2c) displayed infinite 1-dimensional [2..._∞] rows that are formed by intermolecular sp³-C...O interactions (see Figure S7 for the packing in the other two dimensions). The observed intermolecular distances of 3.017(7) Å (O1...C3) and 3.027(7) Å (O1...C2) are up to 0.203 Å shorter than the combined van der Waals radii of C (1.70 Å) and O (1.52 Å) and thus highly indicative of a bonding interaction.^[4b,12,20a,b,28] The atomic coordinates of a [2...2] dimer extracted from the crystal structure ($\Delta E^{\text{BSSE}} = -10.2$ kcal mol⁻¹) could be reproduced fairly accurately with a DFT geometry optimization, which also gave a large interaction energy of $\Delta E^{\text{BSSE}} = -11.0$ kcal mol⁻¹ (see Figure S6c). Moreover, the intermolecular sp³-C...O distances were reproduced with DFT (albeit slightly shorter than observed at 2.977 and 3.022 Å).

The crystal structures and DFT calculations of **1** and **2** thus indicate that the intermolecular nitrile...nitrile interactions observed in **1** can be significantly distorted by other weak crystal packing forces, while the sp³-C...O interactions observed in **2** are strong enough to persist in and direct the crystal packing. This implies that sp³-C...O interactions can be used as a design

feature to engineer crystal structures. To further develop this idea, crystals of **1** and **2** were grown from 1,4-dioxane (see experimental for details). As envisioned, **1** co-crystallized with a dioxane molecule to form the [1...dioxane] crystal structure adduct shown in Figure 3a ($\Delta E^{\text{BSSSE}} = -10.9 \text{ kcal mol}^{-1}$). The observed intermolecular $\text{sp}^3\text{-C}\cdots\text{O}$ distances are up to 0.242 Å shorter than the sum of the van der Waals radii of C and O (C3...O2). This is very similar to the distances observed in the crystal packing of **2** (Figure 2c).

A DFT geometry optimization of [1...dioxane] essentially reproduced the observed atomic constellation in the crystalline state (Figure 3b). The intermolecular $\text{sp}^3\text{-C}\cdots\text{O}$ distances observed in the crystal structure were also preserved and the interaction energy (ΔE^{BSSSE}) was computed at $-10.46 \text{ kcal mol}^{-1}$; nearly identical to the energy obtained for the [2...2] adduct. As is shown in Figure 3c, the [1...dioxane] adducts are packed within the crystal displaying weak nitrile...nitrile and C-H...O interactions.

Crystallization of **2** from 1,4-dioxane also resulted in the formation of a co-crystal and the unit cell of [2...dioxane] shown in Figure 4a again reveals short intermolecular $\text{sp}^3\text{-C}\cdots\text{O}$ distances (up to 0.261 Å van der Waals overlap for C3...O2).

As was expected, infinite 1-dimensional [2_∞] rows are observed in the crystal packing of [2...dioxane] (Figure 4b, with $\Delta E^{\text{BSSSE}} = -10.79 \text{ kcal mol}^{-1}$ for a dimer) that are nearly identical to those seen in the structure of pure **2** (see Figure S8). In [2...dioxane] however, the [2_∞] stacks are spatially separated by bridging dioxane molecules. As is shown in Figure 4c and d, the interactions of dioxane with the C1/C3 and C1/C2 faces of **2** could be accurately reproduced by DFT. The interaction energies are similar at $\Delta E^{\text{BSSSE}} \approx -9.0 \text{ kcal mol}^{-1}$, yet significantly smaller than calculated for [1...dioxane] and [2...2] (about $-11 \text{ kcal mol}^{-1}$). This can be understood by the reduced steric hindrance of the four cyano groups at the C2/C3 face versus the two CH₂ fragments present at the C1/C2 and C1/C3 sides.^[29]

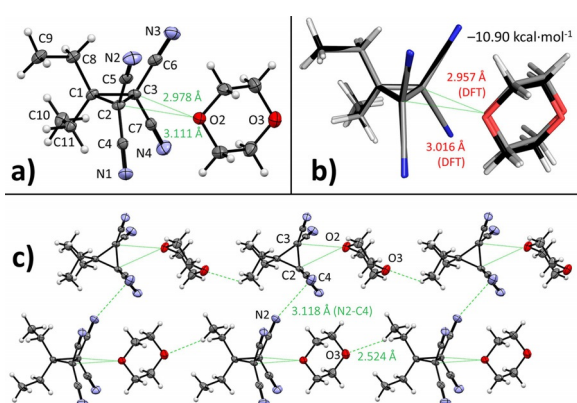


Figure 3. a) Single crystal X-ray diffraction structure of [1...dioxane]. b) structure overlay of [1...dioxane] observed in the crystal structure (carbon in black with $\Delta E^{\text{BSSSE}} = -10.9 \text{ kcal mol}^{-1}$) versus the adduct calculated by DFT at the B3LYP-D3/def2-TZVP level of theory (carbon in grey). The RMSD using only the coordinates of **1** is 0.120 (shown), when using all 39 atoms this value is 0.145. c) crystal packing of the [1...dioxane] adduct. Nitrogen = blue, oxygen = red and hydrogen = white.

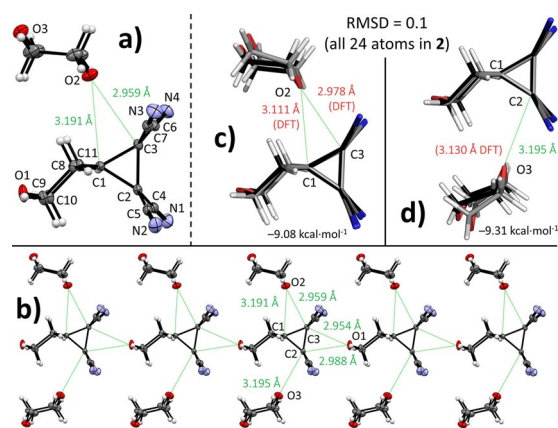


Figure 4. a) Single crystal X-ray diffraction structure of [2...dioxane]; b) Perspective view of an infinite 1D chain of **2**. The chains are separated by the rows of dioxane molecules shown; c) and d) are structure overlays of the [2...dioxane] constellations observed in the crystal structure (carbon in black with calculated ΔE^{BSSSE}) versus those calculated by DFT at the B3LYP-D3/def2-TZVP level of theory (carbon in grey, see also Figure S8). Only intermolecular distances involving the cyclopropane C-atoms are shown. Nitrogen = blue, oxygen = red and hydrogen = white.

When **2** was allowed to crystallize from 1,4-thioxane, [2...thioxane] co-crystals could be isolated and characterized by single crystal X-ray diffraction. As can be seen in Figures 5a and b, this structure is very similar to the dioxane co-crystal (see Figures 4a and b). Again, infinite 1-dimensional [2_∞] rows are observed within the packing (Figure 5b, with $\Delta E^{\text{BSSSE}} = -10.69 \text{ kcal mol}^{-1}$ for a dimer) that are nearly identical to those observed in [2...dioxane] (see Figure S10, bottom). The rows are held together by bridging thioxane molecules, where the thioxane O-atom consistently points towards the C1/C3 face of **2** and an S-atom is directed towards the C1/C2 side of another molecule

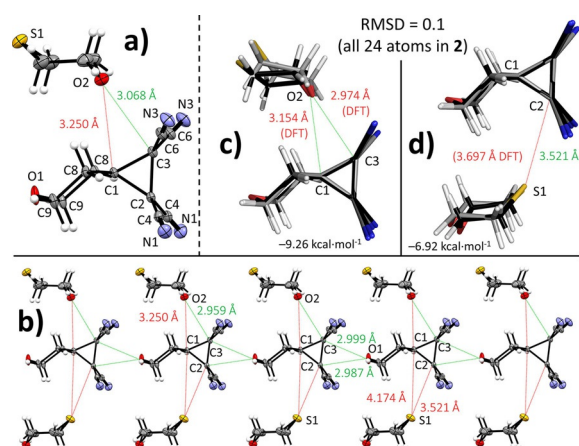


Figure 5. a) Single crystal X-ray diffraction structure of [2...thioxane]; b) Perspective view of an infinite 1D chain of **2**. The chains are separated by the rows of thioxane molecules shown; c) and d) are structure overlays of the [2...thioxane] constellations observed in the crystal structure (carbon in black with calculated ΔE^{BSSSE}) versus those calculated by DFT at the B3LYP-D3/def2-TZVP level of theory (carbon in grey). Only intermolecular distances involving the cyclopropane C-atoms are shown. Distances in green indicate van der Waals overlap, distances in red indicate van der Waals shells are not overlapping. Nitrogen = blue, oxygen = red and hydrogen = white.

of **2**. Two $[2_{\infty}]$ rows are about 0.2 Å further apart in the thioxane versus the dioxane co-crystals and the rows are also shifted by about 0.6 Å with respect to each other (see Figure S10). As can be seen in Figure 5 c and d, the O...**2** and S...**2** constellations of $[2\cdots\text{thioxane}]$ could be reproduced by DFT. The interaction of thioxane-O with the C1/C3 side of **2** (Figure 5 c) has an interaction energy of $\Delta E^{\text{BSSE}} = -9.26 \text{ kcal mol}^{-1}$, which is nearly identical to the energy calculated for a similar constellation in $[2\cdots\text{dioxane}]$ (Figure 4 c). The interaction of thioxane-S with the C1/C2 side of **2** (Figure 5 c) is about $2.3 \text{ kcal mol}^{-1}$ less favourable ($-6.92 \text{ kcal mol}^{-1}$).

Other orientations of the thioxane S-atom near C1/C3 or near C2/C3 all gave about 2 kcal mol^{-1} less stable adduct than for the dioxane analogues (see Figure S11). This implies that the $\text{sp}^3\text{-C}$ -atoms in **2** are more oxophilic than thiophilic.

It is interesting to note that the smaller O ($r_{\text{vdW}} = 1.52 \text{ Å}$) is found at the sterically most accessible C1/C3 face of **2**, while the larger S ($r_{\text{vdW}} = 1.8 \text{ Å}$) is located near the sterically more crowded C1/C2 face of **2** (see Figure S12 for representation of the sterics). This implies that the orientation of the thioxane molecules in-between the $[2_{\infty}]$ rows is driven by $\text{sp}^3\text{-C}\cdots\text{O}$ interactions, and is not directed by a packing that minimizes steric hindrance. This observation further supports that the $\text{sp}^3\text{-C}$ -atoms in **2** are more oxophilic than thiophilic.

The Hirshfeld surfaces of **1** and **2** in all crystal structures were also computed using CrystalExplorer 17.5 and the relevant interaction energies were estimated at the DFT/B3LYP/6-31G level of theory (Figure S13).^[30] These analyses also revealed that the main interactions in the crystal packing involve the $\text{sp}^3\text{-C}(\text{CN})_2$ atoms, with interaction energies generally in line with the ΔE^{BSSE} energy values mentioned above.

To probe the physical nature of the observed $\text{sp}^3\text{-C}\cdots\text{O}$ interactions and to place them into context, several supramolecular adducts of 1,4-dioxane were selected for comparative computational scrutiny. Besides **1** as tetrel bond donor, we selected BMe_3 as a prototypical Lewis acid, Br_2 as a halogen bond donor and H_2O as the prototypical hydrogen bond donor. The molecular representations and interaction energies (ΔE^{BSSE}) of the adducts that were optimized at the B3LYP^[24]-D3^[25]/def2-TZVP^[26] level of theory are collected in Figure 6. Also shown are the results of a non-covalent interaction analysis^[31] and a Morokuma-Ziegler inspired energy decomposition analysis (bottom).^[15b,32]

The interaction energy of $[1\cdots\text{dioxane}]$ is clearly most stabilizing at $-10.5 \text{ kcal mol}^{-1}$. The Lewis acid adduct $[\text{Me}_3\text{B}\cdots\text{dioxane}]$ comes second with $\Delta E^{\text{BSSE}} = -8.0 \text{ kcal mol}^{-1}$, while the halogen bond complex $[\text{Br}_2\cdots\text{dioxane}]$ and the hydrogen-bonded water adduct are least stable with $\Delta E^{\text{BSSE}} \approx -7 \text{ kcal mol}^{-1}$. The energy decomposition analysis revealed that in all cases, the electrostatic component dominates the interaction by contributing 46–58%. In $[1\cdots\text{dioxane}]$ the dispersive interactions are the second largest contributor at 35% and orbital interactions contribute least with 15%. These proportions between dispersion and orbital interactions are the reverse in the other adducts. This can be rationalized considering that energy contributions from dispersive forces scale with contact area,^[33] of which the $[1\cdots\text{dioxane}]$ adduct has the most. The larger contact area (i.e. dispersion) might also explain the increased stability calculated for $[1\cdots\text{dioxane}]$. Likewise, the electrostatic and orbital interactions might well be enhanced in the adduct with **1** because the contact is effectively established with two instead of one Lewis acidic atom(s).

The NCI plots shown at the top of Figure 6 reveal that the electrostatic attraction (blue) always involves a dioxane O-atom and that the region of this attraction roughly coincides with $\text{sp}^3\text{-C}\cdots\text{O}$, $\text{Me}_3\text{B}\cdots\text{O}$, $\text{Br}\cdots\text{O}$ or $\text{HO}\cdots\text{O}$ bonding interactions. Moreover, it is clear from these plots that the dispersive interactions (yellow/green) are significant and decrease in the order $1 > \text{Me}_3\text{B} > \text{Br}_2 \approx \text{H}_2\text{O}$.

Although the significance of *intermolecular* bond critical points (BCPs) in Bader's atoms-in-molecules (AIM) analysis^[34] has been questioned,^[35] we also performed an AIM analysis of the adducts shown in Figure 6 and observed the anticipated^[36] C/B/Br/H...O BCPs (see Figure S14).

All these theoretical analyses thus point at the striking similarities between the physical origins and magnitude of $\text{sp}^3\text{-C}$ centred tetrel bonding interactions with TCCP derivatives and other prototypical electropositive partners.

Summary and Concluding Remarks

In summary, this work provides access to designed $\text{sp}^3\text{-C}$ centred tetrel bond synthons through targeted synthesis of **1** and **2**. These systems were designed to direct their crystal packing by utilizing polar $\text{sp}^3\text{-C}\cdots\text{O}$ interactions. The cyclopropane synthon prefers to interact with sp^3 oxygen over sp^3 sulfur, as evi-

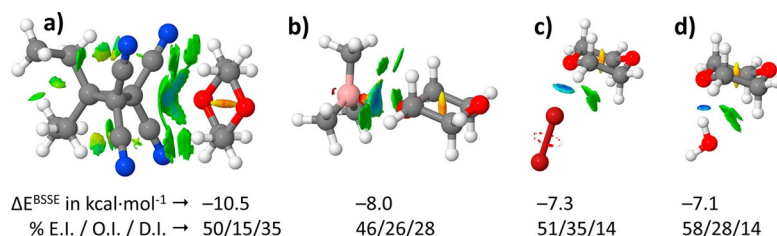


Figure 6. The 'non-covalent interaction' (NCI) analysis of geometry optimized structures, together with the interaction energies (ΔE^{BSSE}) and an energy decomposition analysis of 1,4-dioxane forming: a) sp^3 tetrel-bonding interactions with cyclopropane **1**; b) traditional Lewis acid/base interaction with trimethylborane; c) halogen bonding interactions with molecular bromine; and d) hydrogen bonding to water. Calculations were performed at the B3LYP-D3/def2-TZVP level of theory. In the NCI plots red and yellow = steric repulsion, green = dispersion and blue = electrostatic attraction. Carbon = grey, nitrogen = blue, oxygen = red and hydrogen = white. E.I., O.I. and D.I. stand for, respectively, electrostatic-, orbital-, and dispersion interactions.

denced by the [2...thioxane] co-crystal. DFT calculations indicate interaction energies of up to -11.0 kcal mol $^{-1}$. A diverse range of computational analyses show that the electropositive sp^3 -C $_2$ (CN) $_4$ pockets in **1** and **2** can be seen as a strongly directional 'tetrel-bond donor', similar to halogen bond- or hydrogen bond donors. These results thus demonstrate that 'non-covalent sp^3 -C centred tetrel bonding interactions' can be used to engineer structures in the crystal state. This disclosure has implications for the potential utility of tetrel bond donors like as **1** and **2** in molecular disciplines such as crystal engineering, supramolecular chemistry, molecular recognition and medicinal chemistry.

Experimental Section

Materials and methods: All commercially available chemicals were purchased from Sigma–Aldrich and used without further purification. Solvents were utilized as supplied. 1 H-, 13 C-, and 2D-NMR spectra were acquired at 298 K on a Varian VNMR S500a. Chemical shifts (δ) are reported in parts per million (p.p.m.). Residual solvent resonances were used as internal reference for δ -values in 1 H-, and 13 C-NMR. The FT-IR spectra were measured on a Shimadzu MIRacle 10 single reflection ATR with an IRAffinity-1S Fourier transform infrared spectrophotometer. Field desorption (FR+eFii) mass spectra were recorded on an Advion (T)LC-MS expression LCMS mass spectrometer (with a TLC plate express and isocratic pump).

X-ray intensities were measured on a Bruker D8 Quest Eco diffractometer equipped with a Triumph monochromator ($\lambda = 0.71073$ Å) and a CMOS Photon 50 detector at a temperature of 150(2) K. Intensity data were integrated with the Bruker APEX2 software.^[37] Absorption correction and scaling was performed with SADABS.^[38] The structures were solved using intrinsic phasing with the program SHELXT.^[37] Least-squares refinement was performed with SHELXL-2013^[39] against F^2 of all reflections. Non-hydrogen atoms were refined with anisotropic displacement parameters. The H atoms were placed at calculated positions using the instructions AFIX 13, AFIX 43 or AFIX 137 with isotropic displacement parameters having values 1.2 or 1.5 times U_{eq} of the attached C atoms. Deposition Number(s) 1990043, 1990044, 1990045, 1990046, 1990047, 1990048 contain(s) the supplementary crystallographic data for this paper. These data are provided free of charge by the joint Cambridge Crystallographic Data Centre and Fachinformationszentrum Karlsruhe Access Structures service www.ccdc.cam.ac.uk/structures.

The graphical rendering of the crystal structures has C, N, O and S atoms represented as thermal ellipsoids drawn at 50% probability and hydrogen atoms drawn as spheres with 0.15 Å radius.

DFT geometry optimization calculations were performed with Spartan 2016 at the B3LYP^[24]-D3^[25]/def2-TZVP^[26] level of theory, which is known to give accurate results at reasonable computational cost and a very low basis set superposition error (BSSE).^[25–26] The molecular fragments were manually oriented in a suitable constellation before starting an unconstrained geometry optimization. The Amsterdam Density Functional (ADF)^[32a] modelling suite at the B3LYP^[24]-D3^[25]/TZ2P^[26] level of theory (no frozen cores) was used to compute the reported BSSE corrected energies (ΔE^{BSSE} , using the 'ghost atoms' option for counterpoise correction) of the optimized structures as well as the adducts observed in the crystal structures. ADF was likewise used to compute the energy decomposition and 'atoms in molecules'^[34] analyses (using the default ADF settings). Details of the Morokuma-Ziegler inspired energy decomposition

Scheme used in the ADF-suite have been reported elsewhere^[32a,b] and the Scheme has proven useful to evaluate hydrogen bonding interactions.^[15b,32c] The NCI analysis was performed with AIMAll (version 19.10.12, available at aim.tkgristmill.com) using the defaults settings: surface cut-off = 0.5 a.u.; cut-off to remove covalent density = 0.05 a.u.; colour isosurface range = ± 0.04 a.u. CrystalExplorer 17.5 (<https://crystalexplorer.scb.uwa.edu.au>) was used to compute Hirshfeld surfaces and estimate interaction energies in the crystal structures (see Figure S14).^[30]

Structure overlays of atomic coordinates were fitted with the pair fitting function of PyMOL, by minimizing the Root Mean Square Deviation (RMSD) between two (selected) sets of atomic coordinates.

3,3-diethyl-1,1,2,2-tetracyanocyclopropane (1): A 500 mL round-bottom was charged with, respectively, a magnetic stirrer, ethanol (60 mL), malononitrile (5.9514 g, 90 mmol), NaOAc (0.7378 g, 9 mmol) and 3-pentanone (3.2 mL, 30 mmol). The colourless solution was heated under reflux for 30 minutes. To the brown solution, 150 mL of a 0.2 M solution of an aqueous bromine (1.56 mL, 30 mmol) solution was added using a dropping funnel. During the addition of bromine, a precipitate formed and the mixture darkened. The mixture was stirred at room temperature overnight. The dark brown mixture was vacuum filtered and thoroughly washed first with water and then with ice-cold ethanol. The residue was 1.993 g (10.1 mmol, 34% yield) of a white crystalline powder analysed as **1**. Crystals suitable for SC-XRD could be grown by slow diffusion from dichloromethane and from 1,4-dioxane. **Physical data** (see Figure S1 and S2 for NMR and IR spectra, respectively): 1 H NMR (500 MHz; [D $_6$]DMSO) $\delta = 1.85$ (q, $^3J_{\text{HH}} = 20$ Hz, 4H, CH $_2$), 1.12 (t, $^3J_{\text{HH}} = 10$ Hz, 6H, CH $_3$) p.p.m.; 13 C NMR (126 MHz; [D $_6$]DMSO) $\delta = 109.8$ (CN), 48.0 (C(CN) $_2$), 27.3 (C(Et) $_2$), 22.8 (CH $_2$), 8.6 (CH $_3$) p.p.m.; FT-IR (neat, main peaks) $\nu = 2900$ –3000 (w, C–H stretch), 2255 (m, C \equiv N stretch), 1470, 1456 (s, C–H bending), 1123–948 (m, various C–C and C–H rock and stretch), 801, 727, 669 (s, C–C rock and stretch) cm $^{-1}$; HRMS (FD): m/z found (calcd) for [C $_{11}$ H $_{10}$ N $_4$] $^+$: 198.0830 (198.0905). SC-XRD (from dichloromethane) of C $_{11}$ H $_{10}$ N $_4$, $F_w = 198.23$, colourless block, 0.711 \times 0.334 \times 0.321 mm, monoclinic, $P2_1/n$ (No: 14), $a = 11.6118(7)$, $b = 6.7528(4)$, $c = 14.2042(8)$ Å, $\alpha = 90$, $\beta = 104.184(2)$, $\gamma = 90$ °, $V = 1079.83(11)$ Å 3 , $Z = 4$, $D_x = 1.219$ g cm $^{-3}$, $\mu = 0.078$ mm $^{-1}$. 28447 Reflections were measured up to a resolution of (sin θ/λ) $_{\text{max}} = 0.6$ Å $^{-1}$. 5208 Reflections were unique ($R_{\text{int}} = 0.0339$), of which 4092 were observed [$I > 2\sigma(I)$]. 138 Parameters were refined with 0 restraints. $R1/wR2$ [$I > 2\sigma(I)$]: 0.0482/0.1121. $R1/wR2$ [all refl.]: 0.0683/0.1245. $S = 1.048$. Residual electron density between 0.431 and -0.223 eÅ $^{-3}$. CCDC 1990048. SC-XRD (from 1,4-dioxane) of C $_{15}$ H $_{18}$ N $_4$ O $_2$, $F_w = 286.33$, colourless block, 0.53 \times 0.237 \times 0.161 mm, monoclinic, Cc (No: 9), $a = 10.9559(6)$, $b = 20.9754(12)$, $c = 8.3074(4)$ Å, $\alpha = 90$, $\beta = 125.563(2)$, $\gamma = 90$ °, $V = 1552.99(15)$ Å 3 , $Z = 4$, $D_x = 1.225$ g cm $^{-3}$, $\mu = 0.084$ mm $^{-1}$. 31827 Reflections were measured up to a resolution of (sin θ/λ) $_{\text{max}} = 0.84$ Å $^{-1}$. 2726 Reflections were unique ($R_{\text{int}} = 0.0579$), of which 2459 were observed [$I > 2\sigma(I)$]. 193 Parameters were refined with 2 restraints. $R1/wR2$ [$I > 2\sigma(I)$]: 0.0446/0.0977. $R1/wR2$ [all refl.]: 0.0536/0.1014. $S = 1.149$. Residual electron density between 0.175 and -0.185 eÅ $^{-3}$. CCDC 1990044.

6-oxa-1,1,2,2-tetracyanospiro[2.5]octane (2): A 100 mL round-bottom was charged with, respectively, a magnetic stirrer, ethanol (20 mL), malononitrile (1.6606 g, 30 mmol) and NaOAc (0.2459 g, 3 mmol). Upon addition of tetrahydro-4H-pyran-4-one (0.93 mL, 10 mmol), a white precipitate was formed, which dissolved when the mixture was heated under reflux for 30 minutes. To the brown solution, 50 mL of a 0.2 M solution of an aqueous bromine (0.52 mL, 10 mmol) solution was added using a dropping funnel.

During the addition of bromine, a precipitate formed. The mixture was stirred under reflux overnight, after which it was cooled to laboratory temperature and filtrated using a Büchner funnel. Vacuum drying of the solid gave 1.231 g (5.80 mmol, 58% yield) of a white crystalline powder analysed as **2**. Crystals suitable for SC-XRD could be grown by slow diffusion from dichloromethane, acetonitrile and from 1,4-dioxane. **Physical data** (see Figure S3 and S4 for NMR and IR spectra, respectively): ^1H NMR (500 MHz; $[\text{D}_6]\text{DMSO}$) δ = 3.82 (bs, 4H, OCH_2CH_2), 1.96 (bs, 4H, OCH_2CH_2) p.p.m.; ^{13}C NMR (126 MHz; $[\text{D}_6]\text{DMSO}$) δ = 109.6 (CN), 63.7 (OCH_2CH_2), 43.3 ($\text{C}(\text{CN})_2$), 29.3 (OCH_2CH_2), 26.9 ($\text{C}(\text{CH}_2)_2$) p.p.m.; FT-IR (neat, main peaks) ν = 2900–3000 (w, C–H stretch), 2255 (m, $\text{C}\equiv\text{N}$ stretch), 1422–1230 (w, C–H and C–C stretch/bends), 1092 (s, C–O stretch), 1026, 1009, 984, 941, 841, 729 (m, various C–C and C–O rock and stretch) cm^{-1} ; HRMS (FD): m/z found (calcd) for $[\text{C}_{11}\text{H}_8\text{N}_4\text{O}]^+$: 212.0702 (212.0698). SC-XRD (from dichloromethane) of $\text{C}_{11}\text{H}_8\text{N}_4\text{O}$, Fw = 212.21, colourless block, $0.186 \times 0.152 \times 0.111$ mm, monoclinic, Pn (No: 7), a = 6.9636(10), b = 11.4508(15), c = 7.0277(10) Å, α = 90, β = 114.125(4), γ = 90°, V = 511.43(12) Å³, Z = 2, D_x = 1.378 g cm^{-3} , μ = 0.095 mm^{-1} . 9428 Reflections were measured up to a resolution of $(\sin \theta/\lambda)_{\text{max}}$ = 0.84 Å⁻¹. 1809 Reflections were unique (R_{int} = 0.0672), of which 1464 were observed [$I > 2\sigma(I)$]. 146 Parameters were refined with 2 restraints. R1/wR2 [$I > 2\sigma(I)$]: 0.0559/0.0986. R1/wR2 [all refl.]: 0.0811/0.1053. S = 1.077. Residual electron density between 0.234 and -0.19 e Å^{-3} . CCDC 1990043. SC-XRD (from acetonitrile) of $\text{C}_{11}\text{H}_8\text{N}_4\text{O}$, Fw = 212.21, colourless block, $1.167 \times 0.393 \times 0.258$ mm, monoclinic, Pn (No: 7), a = 6.9428(5), b = 11.4157(9), c = 7.0013(6) Å, α = 90, β = 114.155(2), γ = 90°, V = 506.32(7) Å³, Z = 2, D_x = 1.392 g cm^{-3} , μ = 0.096 mm^{-1} . 11811 Reflections were measured up to a resolution of $(\sin \theta/\lambda)_{\text{max}}$ = 0.77 Å⁻¹. 2299 Reflections were unique (R_{int} = 0.0375), of which 2214 were observed [$I > 2\sigma(I)$]. 146 Parameters were refined with 2 restraints. R1/wR2 [$I > 2\sigma(I)$]: 0.041/0.1012. R1/wR2 [all refl.]: 0.0432/0.1024. S = 1.173. Residual electron density between 0.242 and -0.177 e Å^{-3} . CCDC 1990046. SC-XRD (from 1,4-dioxane) of $\text{C}_{15}\text{H}_{16}\text{N}_4\text{O}_3$, Fw = 300.32, colourless block, $0.335 \times 0.3 \times 0.224$ mm, monoclinic, $P2_1/c$ (No: 14), a = 13.1886(9), b = 6.9180(5), c = 17.5471(11) Å, α = 90, β = 110.051(2), γ = 90°, V = 1503.94(18) Å³, Z = 4, D_x = 1.326 g cm^{-3} , μ = 0.095 mm^{-1} . 49100 Reflections were measured up to a resolution of $(\sin \theta/\lambda)_{\text{max}}$ = 0.8 Å⁻¹. 3072 Reflections were unique (R_{int} = 0.0302), of which 2769 were observed [$I > 2\sigma(I)$]. 199 Parameters were refined with 0 restraints. R1/wR2 [$I > 2\sigma(I)$]: 0.0484/0.1381. R1/wR2 [all refl.]: 0.0539/0.142. S = 1.154. Residual electron density between 0.362 and -0.248 e Å^{-3} . CCDC 1990045. SC-XRD (from 1,4-thioxane) of $\text{C}_{15}\text{H}_{16}\text{N}_4\text{O}_2\text{S}$, Fw = 316.38, colourless plate, $0.528 \times 0.375 \times 0.22$ mm, orthorhombic, $Pnma$ (No: 62), a = 17.9218(14), b = 12.4693(10), c = 6.9617(5) Å, α = 90, β = 90, γ = 90°, V = 1555.7(2) Å³, Z = 4, D_x = 1.351 g cm^{-3} , μ = 0.221 mm^{-1} . 50993 Reflections were measured up to a resolution of $(\sin \theta/\lambda)_{\text{max}}$ = 0.6 Å⁻¹. 3886 Reflections were unique (R_{int} = 0.0452), of which 3346 were observed [$I > 2\sigma(I)$]. 109 Parameters were refined with 0 restraints. R1/wR2 [$I > 2\sigma(I)$]: 0.0605/0.1358. R1/wR2 [all refl.]: 0.0713/0.1415. S = 1.15. Residual electron density between 0.688 and -0.577 e Å^{-3} . CCDC 1990047.

Acknowledgements

TJM thanks NWO (VIDI project 723.015.006) for funding and AF gratefully acknowledges MICIU/AEI from Spain for financial support (project number CTQ2017-85821-R, FEDER funds). Open access funding enabled and organized by Projekt DEAL.

Conflict of interest

The authors declare no conflict of interest.

Keywords: crystal engineering · density functional calculations · small ring systems · $\text{sp}^3\text{-C}$ tetrel bonding interactions · supramolecular chemistry

- [1] a) P. J. Cragg, *Supramolecular Chemistry: From Biological Inspiration to Biomedical Applications*, 1 ed., Springer, Dordrecht, **2010**; b) A. Bauzá, T. J. Mooibroek, A. Frontera, *ChemPhysChem* **2015**, *16*, 2496–2517.
- [2] a) H. J. Schneider, *Supramolecular Systems in Biomedical Fields*, 1 ed., RSC Publishing, Cambridge, UK, **2013**; b) T. Steiner, *Angew. Chem. Int. Ed.* **2002**, *41*, 48–76; *Angew. Chem.* **2002**, *114*, 50–80; c) P. Metrangolo, H. Neukirch, T. Pilati, G. Resnati, *Acc. Chem. Res.* **2005**, *38*, 386–395; d) *Hydrogen Bonding: New Insights*, S. J. Grabowski (ed.), Springer, Heidelberg, **2006**; e) M. R. Scholfield, C. M. Vander Zanden, M. Carter, P. Shing Ho, *Protein Sci.* **2013**, *22*, 139–152.
- [3] a) P. Politzer, J. S. Murray, P. Lane, *Int. J. Quantum Chem.* **2007**, *107*, 3046–3052; b) S. J. Grabowski, *Phys. Chem. Chem. Phys.* **2013**, *15*, 7249–7259; c) S. Scheiner, *Acc. Chem. Res.* **2013**, *46*, 280–288.
- [4] a) R. H. Crabtree, *Chem. Soc. Rev.* **2017**, *46*, 1720–1729; b) A. Bauzá, T. J. Mooibroek, A. Frontera, *Chem. Rec.* **2016**, *16*, 473–487.
- [5] S. Matile, *Chem. Eur. J.* **2019**, *25*, 6460.
- [6] K. Strakova, L. Assies, A. Goujon, F. Piazzolla, H. V. Humeniuk, S. Matile, *Chem. Rev.* **2019**, *119*, 10977–11005.
- [7] S. Benz, J. L. Lopez-Andarias, J. Mareda, N. Sakai, S. Matile, *Angew. Chem. Int. Ed.* **2017**, *56*, 812–815; *Angew. Chem.* **2017**, *129*, 830–833.
- [8] S. Benz, M. Macchione, Q. Verolet, J. Mareda, N. Sakai, S. Matile, *J. Am. Chem. Soc.* **2016**, *138*, 9093–9096.
- [9] a) A. Colom, E. Derivery, S. Soleimanpour, C. Tomba, M. Dal Molin, N. Sakai, M. González-Gaitán, S. Matile, Aurélien Roux, *Nat. Chem.* **2018**, *10*, 1118–1125; b) A. Goujon, A. Colom, K. Strakova, V. Mercier, D. Mahecic, S. Manley, N. Sakai, A. Roux, S. Matile, *J. Am. Chem. Soc.* **2019**, *141*, 3380–3384; c) K. Strakova, A. I. Poblador-Bahamonde, N. Sakai, S. Matile, *Chem. Eur. J.* **2019**, *25*, 14935–14942; d) M. Macchione, A. Goujon, K. Strakova, H. V. Humeniuk, G. Licari, E. Tajkhorshid, N. Sakai, S. Matile, *Angew. Chem. Int. Ed.* **2019**, *58*, 15752–15756; *Angew. Chem.* **2019**, *131*, 15899–15903.
- [10] a) S. J. Grabowski, *Chem. Eur. J.* **2013**, *19*, 14600–14611; b) J. S. Murray, P. Lane, P. Politzer, *J. Mol. Model.* **2009**, *15*, 723–729; c) S. Scheiner, *Chem. Phys. Lett.* **2019**, *714*, 61–64.
- [11] a) P. Murray-Rust, H. B. Bürgi, J. D. Dunitz, *J. Am. Chem. Soc.* **1975**, *97*, 921–922; b) H. B. Bürgi, *Angew. Chem. Int. Ed. Engl.* **1975**, *14*, 460–473; *Angew. Chem.* **1975**, *87*, 461–475; c) M. Harder, B. Kuhn, F. Diederich, *ChemMedChem* **2013**, *8*, 397–404; d) G. J. Bartlett, A. Choudhary, R. T. Raines, D. N. Woolfson, *Nat. Chem. Biol.* **2010**, *6*, 615–620; e) P. H. MacCallum, R. Poet, E. J. Milner-White, *J. Mol. Biol.* **1995**, *248*, 374–384.
- [12] A. Ruigrok van der Werve, Y. R. van Dijk, T. J. Mooibroek, *Chem. Commun.* **2018**, *54*, 10742–10745.
- [13] M. T. Doppert, H. van Overeem, T. J. Mooibroek, *Chem. Commun.* **2018**, *54*, 12049–12052.
- [14] a) Y. P. Zeng, S. W. Sharpe, S. K. Shin, C. Wittig, R. A. Beaudet, *J. Chem. Phys.* **1992**, *97*, 5392–5402; b) A. C. Legon, *Phys. Chem. Chem. Phys.* **2017**, *19*, 14884–14896; c) S. Gao, D. A. Obenchain, J. C. Lei, et al., *Phys. Chem. Chem. Phys.* **2019**, *21*, 7016–7020; d) M. Juanes, R. T. Saragi, W. Caminati, A. Lesarri, *Chem. Eur. J.* **2019**, *25*, 11402–11411; e) J. L. Casals-Sainz, A. C. Castro, E. Francisco, A. Angel-Pendás, *Molecules* **2019**, *24*, 2204.
- [15] a) V. R. Mundlapati, D. K. Sahoo, S. Bhaumik, S. Jena, A. Chandrakar, H. S. Biswal, *Angew. Chem. Int. Ed.* **2018**, *57*, 16496–16500; *Angew. Chem.* **2018**, *130*, 16734–16738; b) T. J. Mooibroek, *Molecules* **2019**, *24*, 3370; c) A. Daolio, P. Scilabra, G. Terraneo, G. Resnati, *Coord. Chem. Rev.* **2020**, *413*, 213265; d) A. Bauzá, A. Frontera, *Crystals* **2016**, *6*, 26.
- [16] a) J. Langer, S. Matejčík, E. Illenberger, *Phys. Chem. Chem. Phys.* **2000**, *2*, 1001–1005; b) J. Mikosch, S. Trippel, C. Eichhorn, R. Otto, U. Lourderaj, J. X. Zhang, W. L. Hase, M. Weidemüller, R. Wester, *Science* **2008**, *319*,

- 183–186; c) S. Pierrefixe, J. Poater, C. Im, F. M. Bickelhaupt, *Chem. Eur. J.* **2008**, *14*, 6901–6911.
- [17] C. B. Aakeroy, D. L. Bryce, G. Desiraju, A. Frontera, A. C. Legon, F. Nicotra, K. Rissanen, S. Scheiner, G. Terraneo, P. Metrangolo, G. Resnati, *Pure Appl. Chem.* **2019**, *91*, 1889–1892.
- [18] a) A. Bauzá, T. J. Mooibroek, A. Frontera, *Angew. Chem. Int. Ed.* **2013**, *52*, 12317–12321; *Angew. Chem.* **2013**, *125*, 12543–12547; b) S. J. Grabowski, *Phys. Chem. Chem. Phys.* **2014**, *16*, 1824–1834.
- [19] That such C-centres are indeed best described as sp^3 hybridised is evident from the Natural Localized Molecular Orbital (NLMO) analysis of dimethyl-TCCP shown in Table S1.
- [20] a) A. Bauzá, T. J. Mooibroek, A. Frontera, *Chem. Eur. J.* **2014**, *20*, 10245–10248; b) A. Bauzá, A. Frontera, T. J. Mooibroek, *Phys. Chem. Chem. Phys.* **2016**, *18*, 1693–1698; c) E. C. Escudero-Adán, A. Bauzá, A. Frontera, A. Frontera, P. Ballester, *ChemPhysChem* **2015**, *16*, 2530–2533.
- [21] V. L. Heywood, T. P. J. Alford, J. J. Roelleveld, S. J. Lekanne Deprez, A. Verhoofstad, J. I. van der Vlugt, S. R. Domingos, M. Schnell, A. P. Davis, T. J. Mooibroek, *Chem. Sci.* **2020**, *11*, 5289–5293.
- [22] a) A. Bauzá, T. J. Mooibroek, A. Frontera, *Phys. Chem. Chem. Phys.* **2014**, *16*, 19192–19197; b) B. Galmés, J. Adrover, G. Terraneo, S. Cardullo, L. J. Gómez Pérez, N. Cellini, M. Sarlo, A. Bonci, L. Gallimberti, *Phys. Chem. Chem. Phys.* **2020**, *22*, 12757–12765.
- [23] Crystals were also grown from acetonitrile, leading to a nearly identical structure (see Figure S6a, with ΔE^{BSSE} of the dimer computed at $-10.95 \text{ kcal mol}^{-1}$).
- [24] a) A. D. Becke, *Phys. Rev. A* **1988**, *38*, 3098–3100; b) C. T. Lee, W. T. Yang, R. G. Parr, *Phys. Rev. B* **1988**, *37*, 785–789.
- [25] S. Grimme, J. Antony, S. Ehrlich, H. Krieg, *J. Chem. Phys.* **2010**, *132*, 154104.
- [26] a) F. Weigend, R. Ahlrichs, *Phys. Chem. Chem. Phys.* **2005**, *7*, 3297–3305; b) F. Weigend, *Phys. Chem. Chem. Phys.* **2006**, *8*, 1057–1065.
- [27] F. H. Allen, O. Kennard, D. G. Watson, L. Brammer, A. Guy Orpen, R. Taylor, *J. Chem. Soc., Perkin Trans. 2* **1987**, S1–S19.
- [28] A. Bondi, *J. Phys. Chem.* **1964**, *68*, 441–452.
- [29] In all observed cases of $sp^3\text{-C}\cdots\text{O}$ interactions, the cyclopropane ring is perpendicular to the plane of the O-donating cyclic ether. The con-
lations where both rings are coplanar were calculated to be about $0.5\text{--}1.1 \text{ kcal mol}^{-1}$ higher in energy than the observed perpendicular arrangements (see Figure S9).
- [30] a) M. A. Spackman, J. J. McKinnon, *Crystengcomm* **2002**, *4*, 378–392; b) J. J. McKinnon, M. A. Spackman, A. S. Mitchell, *Acta Crystallogr. Sect. B* **2004**, *60*, 627–668; c) M. A. Spackman, D. Jayatilaka, *Crystengcomm* **2009**, *11*, 19–32; d) C. F. Mackenzie, P. R. Spackman, D. Jayatilaka, M. A. Spackman, *IUCrJ* **2017**, *4*, 575–587; e) M. J. Turner, S. Grabowsky, D. Jayatilaka, M. A. Spackman, *J. Phys. Chem. Lett.* **2014**, *5*, 4249–4255.
- [31] J. Contreras-García, E. R. Johnson, S. Keinan, R. Chaudret, J.-P. Piquemal, D. N. Beratan, W. Yang, *J. Chem. Theory Comput.* **2011**, *7*, 625–632.
- [32] a) G. te Velde, F. M. Bickelhaupt, E. J. Baerends, C. Fonseca Guerra, S. J. A. van Gisbergen, J. G. Snijders, T. Ziegler, *J. Comput. Chem.* **2001**, *22*, 931–967; b) F. M. Bickelhaupt, E. J. Baerends, *Reviews in Computational Chemistry, Vol. 15* (Eds.: K. B. Lipkowitz, D. B. Boyd), Wiley, New York, **2000**, pp. 1–86; c) S. C. C. van der Lubbe, C. Fonseca Guerra, *Chem. Asian J.* **2019**, *14*, 2760–2769.
- [33] *Physical Chemistry*, 10 ed. (Eds.: P. W. Atkins, J. de Paula), Oxford University Press, Oxford, **2014**, pp. 673–674.
- [34] R. F. W. Bader, *Acc. Chem. Res.* **1985**, *18*, 9–15.
- [35] C. R. Wick, T. Clark, *J. Mol. Model.* **2018**, *24*, 9.
- [36] a) E. Espinosa, E. Molins, C. Lecomte, *Chem. Phys. Lett.* **1998**, *285*, 170–173; b) M. V. Vener, A. N. Egorova, A. V. Churakov, V. G. Tsirelson, *J. Comput. Chem.* **2012**, *33*, 2303–2309; c) I. Mata, I. Alkorta, E. Espinosa, E. Molins, *Chem. Phys. Lett.* **2011**, *507*, 185–189; d) A. Bauzá, A. Frontera, *ChemPhysChem* **2020**, *21*, 26–31.
- [37] Bruker, *APEX2 software*, USA, Madison WI, **2014**.
- [38] G. M. Sheldrick, *SADABS*, Germany, Universität Göttingen, **2008**.
- [39] G. M. Sheldrick, *SHELXL2013*, Germany, Universität Göttingen, **2013**.

Manuscript received: May 28, 2020

Revised manuscript received: June 16, 2020

Accepted manuscript online: June 18, 2020

Version of record online: July 20, 2020